Rapid Communications

Origin of the dramatic change of fission mode in fermium isotopes investigated using Langevin equations

Y. Miyamoto,[1] Y. Aritomo,[1] S. Tanaka,[1] K. Hirose,[2] and K. Nishio[2]
[1]*Faculty of Science and Engineering, Kindai University, Higashi-Osaka, Japan*
[2]*Advanced Science Research Center, Japan Atomic Energy Agency, Tokai, Ibaraki, Japan*

(Received 18 February 2018; revised manuscript received 17 January 2019; published 14 May 2019)

The fission of even-even fermium nuclides $^{250-260}$Fm at low excitation energy was studied using Langevin equations of three-dimensional nuclear-shape parametrization. The mass distributions of fission fragments show a dramatic change from an asymmetric shape for the lighter fermium isotopes to sharp symmetric fission for the heavier isotopes. The time evolution of the nuclear shape on the potential surface reveals that the lighter fermium isotopes showing asymmetric fission are trapped in the second minimum for a substantial length of time before overcoming the second saddle point. This behavior changes dramatically for the compact symmetric fission found in the heavier neutron-rich fermium nuclei that disintegrate immediately after overcoming the first saddle point, without feeling the second barrier, resulting in a fission time two orders of magnitude shorter.

DOI: 10.1103/PhysRevC.99.051601

Nuclear fission is a fundamental phenomenon that is used to generate energy in atomic power plants. Furthermore, as a neutron source supplied by dedicated nuclear reactors, fission provides many applications for science and industry. Understanding of the fission process itself has a large impact on other fields of science. Partial half-lives for spontaneous fission (sf), for example, influence the limit of existence of super-heavy nuclei. Recently, the fission of very neutron-rich nuclei, occurring in the *r*-process nucleosynthesis, is being discussed in order to explain the abundance peaks [1].

Owing to the complex nature of the fission process, many phenomena have not yet been elucidated, even though almost 80 years have passed since its discovery [2,3]. One of the biggest challenges is to clarify the dramatic change of the fission-fragment mass distributions (FFMDs) in the fermium (atomic number $Z = 100$) region. In contrast to the mass-asymmetric fission for typical actinide nuclides, a sharp mass-symmetric FFMD emerges in neutron-rich heavy actinides following the addition of just one extra neutron, e.g., from asymmetric fission of ^{257}Fm to sharp symmetric fission of ^{258}Fm [4,5]. A qualitative interpretation of the sharp mass-symmetric fission is that two identical nuclei in the vicinity of the doubly magic nucleus ^{132}Sn are generated at the instance of nuclear rupture (scission). This idea is also supported by the large total kinetic energy (TKE) and the smaller neutron multiplicity in symmetric fission, indicative of a compact configuration at scission [6–8]. Also, measured FFMDs and TKE distributions are explained only by invoking two independent paths (modes), characterized by sharp symmetric fission with large TKE and broad symmetric fission with small TKE [6].

Long-standing theoretical challenges to elucidating the fermium problem are (i) to unveil different pathways on the potential energy surface leading to different scission configurations and (ii) to explain the mechanism causing such a sudden change of the fission path. In spite of many attempts using elaborate models based on the macroscopic-microscopic model [9–12] or fully microscopic approach [13–19], the reported results examine only a few aspects of fission and do not reach a comprehensive understanding, as mentioned below.

By analyzing a potential energy landscape, two or three fission modes for ^{258}Fm are identified [12,13,15,16,19]. One is the *compact* symmetric fission (cSF). The others are *elongated* asymmetric fission (eAF) and/or *elongated* symmetric fission (eSF). In these models, the dominant fission mode for each fermium nucleus was explained in terms of the structure of the second fission barrier. However, the probabilities leading to each fission mode have not yet been quantified. Concerning the fission observables, such as FFMD and TKE distribution, they are only partially studied so far. FFMD [12] and TKE [18,20] were calculated for ^{258}Fm, but discussed only as one dominant mode, irrespective of the experimentally known multimodal fission of ^{258}Fm. As an alternative approach, fission of fermium nuclides were studied using a scission point model, which predicts fission observables by searching for the optimal configuration at scission with respect to total energy [14,21–23]. Again, the abrupt change of fission properties for fermium isotopes was not reproduced.

In this paper, we performed calculations to challenge the unsolved problem of fermium fissions using a fluctuation-dissipation model (Langevin calculation) [24–31]. Recently, Langevin calculations have been adopted extensively for the study of low-energy fissions [32–44]. An advantage of this semiclassical stochastic model is that fission observables (mass, TKE, and deformation) are generated in an event-by-event basis, by tracking trajectories of a system moving on the potential energy surface. Also, the concept of fission time is automatically introduced. The calculation in Ref. [33] already showed three fission modes in ^{264}Fm, i.e. cSF, eSF, and asymmetric fission. In the low-energy fission of ^{258}Fm, a pronounced peak structure in the FFMD of cSF is well demonstrated in three- [43] and four-dimensional [44] (3D and 4D)

Langevin calculations. In these calculations, however, dramatic change of the FFMDs in the Fm isotopes was not reported. In this work, we attempt to systematically calculate the fission properties across the even-even fermium isotopes using the 3D model [35,36], motivated by a successful description of low-energy fissions for a wide variety of isotopes of Th, Pa, U, Np, and Pu [46,47]. The initial excitation energy of the fissioning nucleus E^* is chosen to be 7.0 MeV as the possible lowest value in the calculation to overcome the fission barrier. Compared to 4D and/or higher-dimension models, our 3D calculation has stricter constraints for the nuclear shape. On the other hand, it requires less computational time, allowing us to gain statistics to investigate, for example, fission modes with small yields.

Although the results do not allow a direct comparison with sf data, an essential mechanism to explain the unique feature of fermium fissions was discovered, including the sudden change of the FFMDs. As well as elucidating the raised questions, i.e., (i) and (ii) mentioned above, the results indicate that the fission times for each mode, cSF and eAF, are remarkably different from each other, by about two orders of magnitude. This could give a hint as to the cause of the sharp drop in the partial half-life for sf from ^{256}Fm to ^{258}Fm (cf. Fig. 10 in [45]).

In our calculation, the nuclear shape is defined by the two-center model [48,49] with the three-dimensional shape parametrization, z, δ, and α [36]. The parameter z corresponds to the distance between two potential centers, δ denotes the deformation of the fragments, and $\alpha = (A_1 - A_2)/(A_1 + A_2)$ is the mass asymmetry of the two fragments, where A_1 and A_2 are the mass numbers of heavy and light fragments [48].

To define the potential of the two-center shell model, a neck parameter of $\epsilon = 0.35$ ($0 \leqslant \epsilon \leqslant 1$) [50] has been routinely used [35,36,38,43,46,47]. Larger values tend to create a narrower neck of the dumbbell-shape nucleus. We found that $\epsilon = 0.35$ cannot reproduce the FFMDs of heavier actinide nuclides, as shown in Fig. 1. For the lightest nucleus, e.g., ^{238}U, the calculated FFMDs are not sensitive to the ϵ value, as discussed in [44]. For heavier isotopes, on the other hand, the distribution is very sensitive to ϵ. The $\epsilon = 0.35$ value, which yields an asymmetric shape for lighter isotopes (e.g., ^{238}U, ^{240}Np, and ^{242}Pu) gives symmetric fissions for heavier nuclides (e.g., ^{248}Cm, ^{250}Bk, and ^{252}Cf). To reproduce the experimental data, the ϵ value was systematically increased with the mass of fissioning nuclides to facilitate the neck formation. A calculation was performed to determine the optimal ϵ values leading to best agreement with each FFMD for $^{237-240}$U, $^{239-242}$Np, and $^{241-243}$Pu, obtained from the multinucleon transfer channels of ^{18}O+^{238}U [47], and $^{247-250}$Cm, $^{249-252}$Bk, $^{251-254}$Cf, from ^{18}O+^{248}Cm [51]. The results of fitted ϵ values are shown in the Supplemental Material [52]. In this process, the optimal ϵ values follow the empirical relation

$$\epsilon(A_c) = 0.01007A_c - 1.94, \quad (1)$$

where A_c is the mass of the fissioning nucleus. The fitted line is shown in [52].

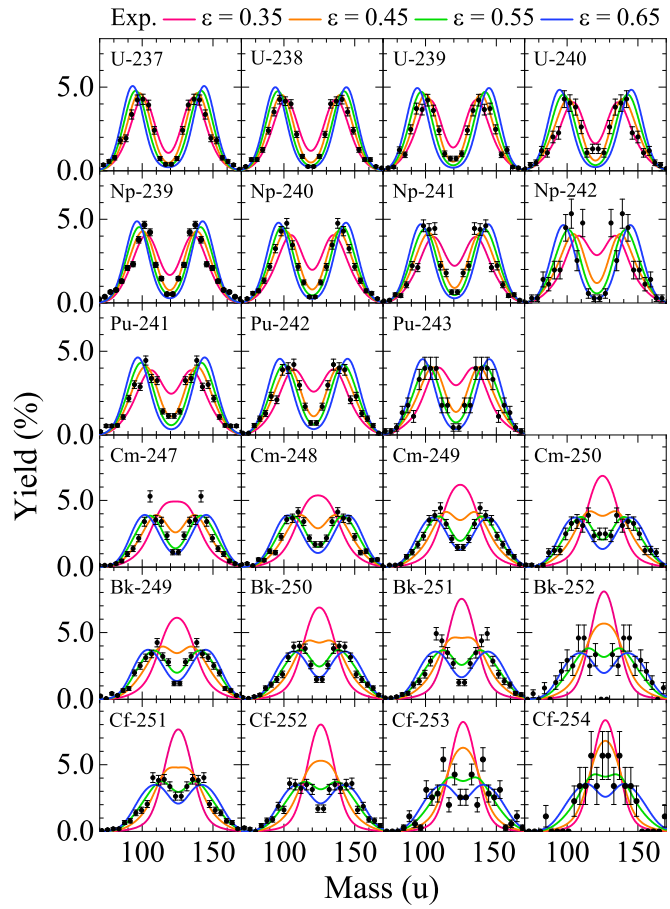

FIG. 1. Fission-fragment mass distributions of several actinide nuclides in the excitation-energy range $E^* = 10 - 20$ MeV (solid circles), obtained via multinucleon-transfer-induced fission [47,51]. Results of Langevin calculations with four selected neck parameters ϵ are shown.

The potential energy of a nucleus $V(z, \delta, \alpha)$ is defined as a sum of the liquid-drop energy $V_{\rm LD}(z, \delta, \alpha)$, calculated with the finite-range liquid-drop model [53], and a microscopic energy correction $E^0_{\rm micro}(z, \delta, \alpha)$. The $E^0_{\rm micro}$ is the sum of the shell correction energy $E^0_{\rm shell}(z, \delta, \alpha)$, evaluated by the Strutinski method [54,55], and the paring energy $E^0_{\rm pair}(z, \delta, \alpha)$ [36].

The excitation-energy dependence of the microscopic energy correction was introduced with the shell-damping energy $E_{\rm d} = 20$ MeV [35,36,56]. The evolution of the nuclear shape with time is calculated by solving the Langevin equations. For more details, see Refs. [35,36].

Figure 2 shows the calculated results of (a) FFMDs, (b) TKE distributions, and (c) mass-TKE correlations for even-even fermium isotopes, $^{250-260}$Fm. In this figure, experimental sf data in the literature for FFMDs and TKE distributions of ^{254}Fm [57], ^{256}Fm [58,59], and ^{258}Fm [6] are shown. The calculated FFMDs for $^{250-254}$Fm show a mass-asymmetric shape with heavy (H) and light (L) fragments centered around $A_{\rm H}/A_{\rm L} \approx 1.47$ ($A_{\rm H} \approx 150$), which is slightly larger than the sf data measured for ^{256}Fm, $A_{\rm H}/A_{\rm L} \approx 1.23$ ($A_{\rm H} \approx 141$) [58]. The overall shape of the FFMDs changes dramatically to sharp symmetric fission for the heavier $^{256-260}$Fm isotopes.

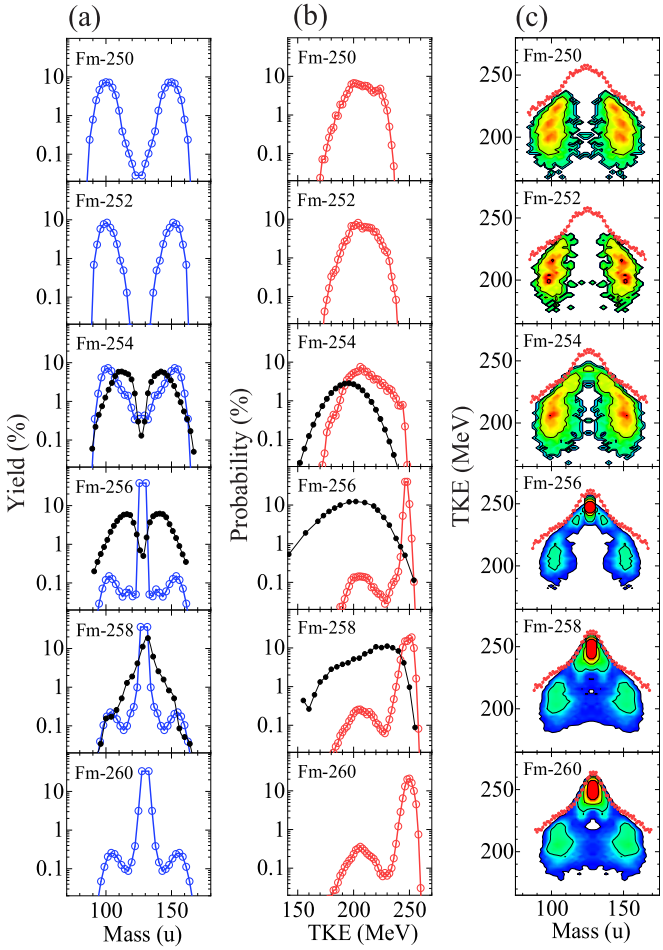

FIG. 2. (a) Fission-fragment mass distributions, (b) total kinetic energy (TKE) distributions, and (c) mass-TKE distributions calculated for six fermium isotopes, $^{250-260}$Fm. Literature data of spontaneous fission for FFMDs (^{254}Fm [57], ^{256}Fm [58], and ^{258}Fm [6]) and TKE distributions (^{254}Fm [57], ^{256}Fm [59], and ^{258}Fm [6]) are shown by black curves connected by solid circles. Solid curves in (c) correspond to the total Q value in fission, $Q_{\rm tot}(A)$ (see text for more details).

One can notice that $^{256-260}$Fm has a small yield showing mass asymmetry $A_{\rm H}/A_{\rm L} \approx 1.50$ ($A_{\rm H} \approx 155$) close to the asymmetric fission of $^{250-254}$Fm.

The results can be explained by multimodal fission, i.e., well-separated fission paths leading to different configurations at scission. The different shapes at the exit of the potential energy surface is demonstrated in the TKE distribution [Fig. 2(b)], calculated as a sum of the Coulomb potential energy at scission and prescission kinetic energy [36]. It is found in the mass-TKE correlation [Fig. 2(c)] that the sharp mass-symmetric fission has a large TKE value E_k ($\bar{E}_k \approx 250$ MeV) with a narrow width, whereas the energetically small ($\bar{E}_k \approx 205$ MeV) and broad TKE distributions are linked to mass-asymmetric fission. The former and the latter modes correspond to cSF and eAF, respectively. The $\bar{E}_k$ value and the width of the TKE distribution for each fission mode can account for the experimental data of ^{258}Fm (sf) [6]. In the Langevin calculation of Refs. [43,44], two fission modes in ^{258}Fm, called super-short and standard following the terminology used by Brosa [10], were also reported with mass-TKE distributions similar to the present results.

Concerning the sharp transition of the FFMDs, the model in [23] also predicted it in terms of the change of the potential energy surface at the scission point. The model, however, does not treat the TKE distribution. The time-dependent density-functional theory showed the TKE distribution and a sharp FFMD for ^{258}Fm [18] that gives better agreement than our model, while isotope dependence of these data is not argued.

What is found in Fig. 2(c) is that the fission of ^{258,260}Fm exhibits a small but non-negligible number of events in the low-TKE and mass-symmetric region. As argued in Refs. [12,15,16,19], we interpret such events as originating from eSF (or super-long [10]). In fact we also confirmed the events as originating from an independent fission mode, by obtaining an increase of the yield with initial excitation energy of the compound nucleus.

In the distribution of fragment mass-TKE correlation shown in Fig. 2(c), the total fission Q value $Q_{\rm tot}(A)$, defined by a sum of the mass difference $Q_{\rm max}(A) = M_{\rm Ac} - (M_{\rm A_L} + M_{\rm A_H})$ [60] and the excitation energy of the compound nucleus $E^* = 7.0$ MeV, are plotted. Here, Q values are chosen to be the largest value around $Z = Z_{\rm c}(A/A_{\rm c})$ with $Z_{\rm c} = 100$ (Fm). All the fission events are located below the $Q_{\rm tot}(A)$ curve, which corresponds to the energetically possible upper limit. It is noteworthy in the fission of ^{256,258,260}Fm that the highest TKE of fragments $E_{\rm k,max}(A)$ in the cSF region agree with the $Q_{\rm tot}(A)$ line. In other words, the mass-TKE distribution for cSF is strongly correlated with the pronounced peak structure of the $Q_{\rm tot}(A)$ curve.

It should be mentioned that the boundary separating asymmetric and symmetric fission is located between $A_{\rm c} = 254$ and 256, two mass units lower than indicated by the available sf data [4]. The difference might imply an inadequate formulation of Eq. (1), arising from the uncertainty $\approx \pm 0.07$ to deduce the ϵ value in each nucleus and a limited number of studied nuclides. Also, we recognize in the TKE distributions for ^{254,256,258}Fm that the peak energies of the calculated spectra are larger than the experimental sf data and the widths are far narrower, both for cSF and eAF. This comes from the larger ϵ parameters adopted to reproduce the experimental FFMDs (see Fig. 1). In the Supplemental Material [52], dependence of the TKE distribution with ϵ is shown for each nucleus. By introducing the larger ϵ values, the calculation deviates from the experimental data for ^{239}Np* (black dots) [61]. For heavier element isotopes, we see complicated dependence of TKE distribution on ϵ. As our experiments carried out in [46,47,51] did not give the TKE distribution with high resolution, we relied only on the FFMD data to confine the ϵ parameter. In spite of the discrepancy, supposedly coming from the limit of the 3D shape parametrization, an important mechanism to change the mass asymmetry over the fermium isotopes was found in the present work.

After reproducing successfully the key fission features of the fermium isotopes with our Langevin calculations, we investigated in greater detail each fission mode by tracking

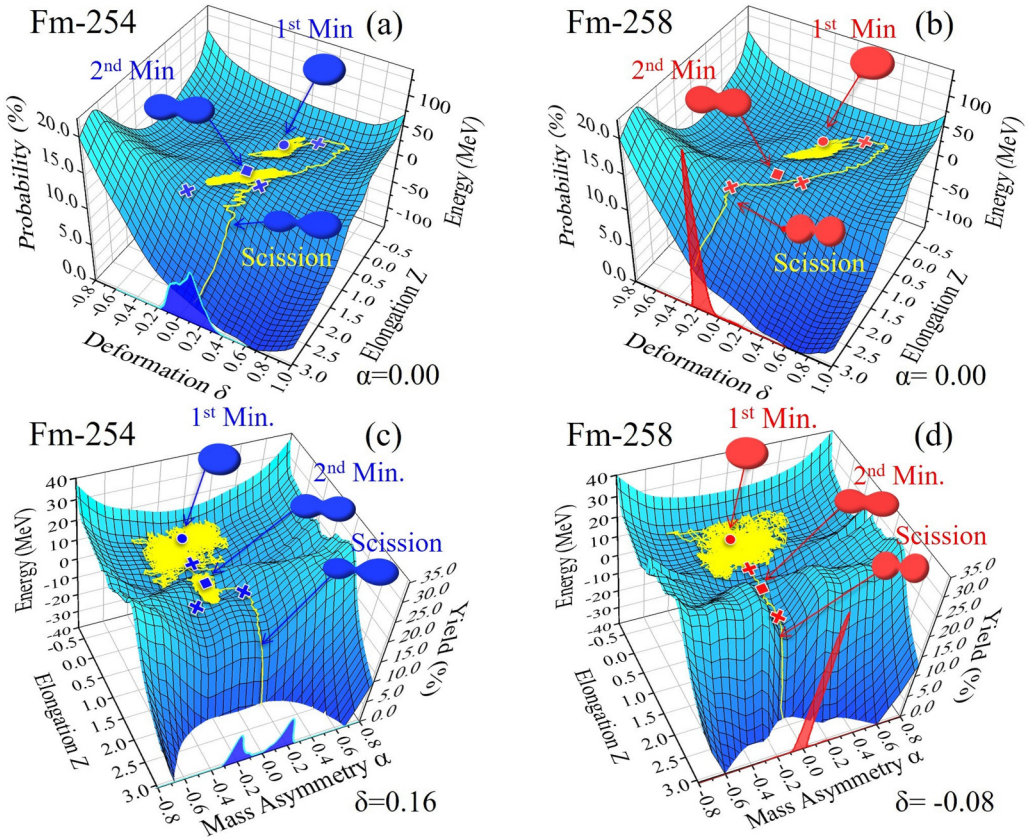

FIG. 3. Potential energy on the z-δ plane for (a) ^{254}Fm and (b) ^{258}Fm, obtained at a fixed mass asymmetry $\alpha = 0$. A sample shape trajectory is shown for each nucleus, selected from those leading to the dominant fission modes, i.e., elongated asymmetric fission (eAF) for ^{254}Fm and compact symmetric fission (cSF) for ^{258}Fm. The trajectories are also shown on the z-α plane for (c) ^{254}Fm and (d) ^{258}Fm as well as the potential energy at a fixed δ value, 0.16 for ^{254}Fm and -0.08 for ^{258}Fm, respectively. Nuclear shapes in each stage of fission trajectory are shown. The ground state (•) and the second minimum (■) as well as the first (+) and the second saddle points (×) are shown. The probability distributions of δ [(a) and (b)] and α [(c) and (d)] values at the scission point are shown for each nucleus, obtained by accumulating all the trajectories from the Langevin calculation.

the shape evolution and finding its correspondence with the potential energy surface. Figures 3(a) and 3(b) show the potential energy V plotted with respect to z and δ at the fixed mass symmetry $\alpha = 0$ for ^{254}Fm and ^{258}Fm, respectively. In each nucleus, one distinctive trajectory that belongs to the predominant mode (eAF for ^{254}Fm and cSF for^{258}Fm), projected on the z-δ plane, is shown, starting from the ground-state minimum. Both systems sustain the shape around the ground-state minimum for a while with characteristic fluctuations originating from the random force in the Langevin equations. The fission process is triggered when the random force drives the system to overcome the first saddle point (+). After crossing over the first saddle point, ^{254}Fm and ^{258}Fm undergo a completely different behavior. ^{254}Fm is trapped in the second minimum, characteristic of the so-called fission isomer, for a substantial time, before escaping from this minimum by passing through the ridge in the vicinity of the second saddle point (×) located on the positive δ side $(z, \delta) = (1.3, 0.2)$. The nucleus then develops its elongation (z) rapidly, leading to the mass-asymmetric scission with the positive δ shape. Figure 3(c) shows the projection of the calculated trajectory of ^{254}Fm on the z-α plane at a fixed deformation $\delta = 0.16$, chosen as a typical value for ^{254}Fm at scission. The nuclear shape fluctuates around the mass-symmetric shape ($\alpha = 0.0$) up to the second minimum. The mass asymmetry in fission is frozen at the instance overcoming the second saddle point and is preserved during the descent from the saddle to scission. Most of the studied trajectories follow a similar behavior after overcoming the first saddle point. However, collective nuclear motion provided in the Langevin equations gives variance of nuclear shape, making the relatively wider distribution in δ [Fig. 3(a)] and α degree of freedom [Fig. 3(c)] at the scission point. It should be noted that ^{254}Fm has another saddle point on the negative δ side $(z, \delta) = (1.8, -0.2)$ as the extreme shape reached by the vibrational motion in the second minimum. The relatively higher energy of the saddle point prevents the system from fissioning in this direction. In the fission of ^{258}Fm, on the contrary, the nucleus does not stagnate around the shape of the second minimum, but disintegrates immediately after overcoming the first saddle point, resulting in cSF. As shown in Fig. 3(b) this is due to the drop of the second barrier of the negative δ side, created by a subtle balance between the macroscopic energy and microscopic shell correction energy. The behavior is

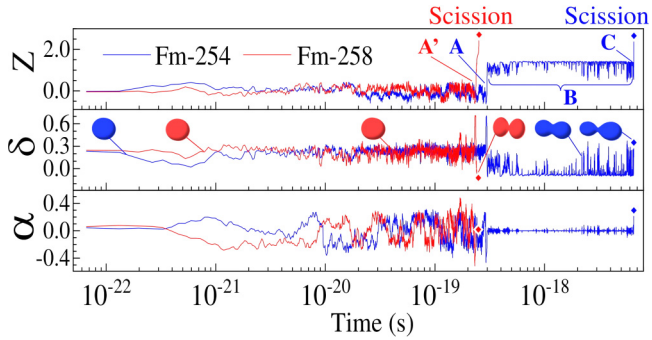

FIG. 4. Evolution of three shape parameters z (top), δ (middle), and α (bottom) with time. The several points indicated by upper-case letters mean: (**A** for ^{254}Fm and **A'** for ^{258}Fm) passing over the fist saddle point, (**B** for ^{254}Fm) trapping period in the second minimum, and (**C** for ^{254}Fm) overcoming the 2nd fission barrier. Scission points are shown by the solid diamonds. Selected nuclear shapes at each stage are shown.

similar to the prediction of [16] that the second fission barrier disappears at ^{258}Fm. The ridge structure in the positive δ side at $(z,\ \delta) = (1.2, 0.2)$ is identified also for ^{258}Fm, similar to ^{254}Fm. However, the probability to overcome this saddle point is very small, because the system must be kicked to a different direction which opposes the dynamical motion in descending the slope, as evidenced in the small fraction of eAF mode (see Fig. 2). From the potential structure and the analysis of several trajectories leading to cSF, it is found that the fluctuation of the shape for ^{258}Fm during the descent from the first saddle point to scission is significantly small, and their trajectories are confined within a narrow deformation window, as seen in the pronounced peak distribution of around $\delta = -0.2$ [Fig. 3(b)] in comparison to the broader distribution for eAF [Fig. 3(a)]. As shown in Fig. 3(d), the limited shape fluctuation is formed by a prominent energy minimum as a fission valley appearing on the energy surface on the z-α plane at $\delta = -0.08$. These features account for the smaller width in its FFMD and TKE distribution, as shown in Fig. 2. It should be also mentioned that the large negative δ value for ^{258}Fm makes the scission-point shape compact [see the nuclear shape inset in Figs. 3(b) and 3(d)]. This results in larger Coulomb potential energy, as the source of larger TKE of postaccelerated fission fragments.

Concerning the mechanism generating the different fission modes, the fissions from the low excited states, as demonstrated in the present calculation, should be the same as the spontaneous fissions. In the fission of ^{240}Pu, the sf [62] has almost similar mass and/or TKE distributions to those from the fission-isomer [63] ($E^* = 2.4$ MeV from the ground state [64]), resonance tunneling [65] (5.1 MeV), and above the barrier [62] (6.53 MeV). These results indicate that fission modes are defined when the system overcomes the second fission barrier, irrespective of initial excited states.

The different fission times between the eAS (^{254}Fm) and the cSF (^{258}Fm) modes can be more exactly examined in Fig. 4, which shows the time t dependence of the shape parameters z, δ, and α. They are the same trajectories shown in Fig. 3. ^{254}Fm overcomes the first saddle point (marked as **A**) at $t \approx 3 \times 10^{-19}$s, then trapped in the second minimum (region **B**) for a long time $\Delta t \approx 6 \times 10^{-18}$s. After getting over the second saddle point **C**, the system scissions quickly with $\Delta t \approx 3 \times 10^{-20}$ s. We stress again that the mass asymmetry in fission for ^{254}Fm is determined only when the system escapes from the second minimum. The averaged overall fission time $t_{\rm fiss}$ from all the trajectory analysis is $\bar{t}_{\rm fiss} = 4 \times 10^{-18}$ s. For the case of ^{258}Fm, the system disintegrates immediately after overcoming the 1st saddle point **A'**. Thus the overall fission time is only $t_{\rm fiss} \approx 2.5 \times 10^{-19}$s. We note that the time from the first saddle to scission for ^{258}Fm $\Delta t \approx 6 \times 10^{-20}$ s is in reasonable agreement with the elapsed time from the exit point of the first barrier of ^{258}Fm to scission, (0.1–1.3) $\times 10^{-20}$ s, obtained recently from the nuclear time-dependent density functional theory [18]. Recent calculation of the saddle-to-scission time for ^{240}Pu [66], $\approx 4 \times 10^{-20}$s, agrees with our results. The averaged fission time $\bar{t}_{\rm fiss} = 5 \times 10^{-20}$ s for ^{258}Fm is about 80 times shorter than the fission of ^{254}Fm.

The difference in fission time between ^{254}Fm and ^{258}Fm reminds us of the sudden drop in the partial half-life for sf $T_{1/2,\rm sf}$ from ^{256}Fm (1.02×10^4 s) to ^{258}Fm ($\approx 0.37 \times 10^{-3}$ s) [45]. A sizable change in $T_{1/2,\rm sf}$ over the fermium isotopes is known to be due to the enhanced stability toward the deformed shells at $(N, Z = (152, 100))$, ^{252}Fm. While $T_{1/2,\rm sf}$ between the neighboring even-even fermium isotopes ($^{246-256}$Fm) change with a factor of $1.5 \times 10^2 - 1.9 \times 10^3$, the significantly huge drop of 2.8×10^7 from ^{256}Fm to ^{258}Fm is widely noticed. Our Langevin calculation shows that the second saddle point does not hinder the fission of the cSF mode in ^{258}Fm, shortening the fission time by about two orders of magnitude compared with the eAF. Assuming that the structure of the second barrier and its impact on the dynamical nuclear motion is also preserved in sf after penetrating the first fission barrier, the sudden drop of $T_{1/2,\rm sf}$ of ^{258}Fm could be attributed to the disappearance of stagnation time in the second minimum, thus, the partial half-life for sf $T_{1/2,\rm sf}$ is solely determined by the tunneling of the first barrier. The lighter fermium isotopes, on the other hand, must penetrate the second barrier. The decreasing importance and/or absence of the second fission barrier of fermium isotopes heavier than ^{256}Fm is also argued in relation to the rapid change of $T_{1/2,\rm sf}$ [13,16]. The present calculation is the first quantitative demonstration that fission time is significantly different between the lighter and heavier Fm isotopes in the fission from the low excited states above the barrier.

To conclude, the fission of even-even fermium isotopes from low excited states was studied using the Langevin equations. The calculated FFMDs and TKE distributions as well as the mass-TKE mapping revealed two competing fission modes. One is the mass-asymmetric fission with large deformation at scission (eAF), that dominates the fission of $^{250-254}$Fm and partially appears in the fission of $^{256-260}$Fm. The other is the sharp mass-symmetric fission with large TKE (cSF), governing the fission of $^{256-260}$Fm. The calculation is the first to demonstrate the experimentally reported dramatic change of the FFMDs in Fm isotopes.

The sudden change of the FFMD and TKE distributions between $^{250-254}$Fm and $^{256-260}$Fm is strongly regulated by

the structure of the second fission barrier and the dynamical motion of the nucleus in the second minimum. In the fission of $^{250-254}$Fm, the systems are trapped in the second minimum for a substantial period of time before overcoming the second saddle point that opens the eAF. The heavier nuclides ($^{256-260}$Fm) lead to cSF immediately after overcoming the first saddle point, without staying in the second minimum, resulting in a fission time two orders of magnitude shorter than eAF. The analysis provides a hint to understanding the sudden decrease of the partial half-life for spontaneous fission from ^{256}Fm to ^{258}Fm.

Note Added in Proof. Recently, mass-TKE distributions for $^{256-259}$Fm were calculated by the 4D Langevin model [67].

The authors are grateful to Prof. M. Ohta of Konan University, and Dr. A. Iwamoto, Dr. M. Asai, Dr. R. Orlandi, Dr. M. J. Vermeulen, Dr. H. Koura, and Dr. Y. Nagame of JAEA for fruitful discussions. Y.M. appreciates the summer student program of JAEA. The Langevin calculations were performed using the cluster computer system (Kindai-VOSTOK) which is supported by Research funds for External Fund Introduction by Kindai University. This work was supported by Japan Society for the Promotion of Science (JSPS) KAKENHI Grant No. 17K05455. Experimental data in Fig. 1 were taken with the support of "Comprehensive study of delayed-neutron yields for accurate evaluation of kinetics of high burn-up reactors" by the Ministry of Education, Culture, Sports, Science and Technology of Japan (MEXT).

[1] M. Eichler *et al.*, Astrophys. J. **808**, 30 (2015).
[2] O. Hahn and F. Straßmann, Naturwissenschaften **27**, 11 (1939).
[3] L. Meitner and O. R. Frisch, Nature (London) **143**, 239 (1939).
[4] D. C. Hoffman and M. R. Lane, Radiochem. Acta **70/71**, 135 (1995).
[5] D. C. Hoffman, G. P. Ford, J. P. Balagna, and L. R. Veeser, Phys. Rev. C **21**, 637 (1980).
[6] E. K. Hulet *et al.*, Phys. Rev. C **40**, 770 (1989).
[7] E. K. Hulet, R. W. Lougheed, J. H. Landrum, J. F. Wild, D. C. Hoffman, J. Weber, and J. B. Wilhelmy, Phys. Rev. C **21**, 966 (1980).
[8] J. F. Wild *et al.*, Phys. Rev. C **41**, 640 (1990).
[9] S. Ćwiok *et al.*, Nucl. Phys. A **491**, 281 (1989).
[10] U. Brosa, S. Großmann, and A. Müller, Phys. Rep. **197**, 167 (1990).
[11] P. Möller, D. G. Madland, A. J. Sierk, and A. Iwamoto, Nature (London) **409**, 785 (2001).
[12] T. Ichikawa, A. Iwamoto, and P. Möller, Phys. Rev. C **79**, 014305 (2009).
[13] M. Warda, J. L. Egido, L. M. Robledo, and K. Pomorski, Phys. Rev. C **66**, 014310 (2002).
[14] N. Dubray, H. Goutte, and J. P. Delaroche, Phys. Rev. C **77**, 014310 (2008).
[15] L. Bonneau, Phys. Rev. C **74**, 014301 (2006).
[16] A. Staszczak, A. Baran, J. Dobaczewski, and W. Nazarewicz, Phys. Rev. C **80**, 014309 (2009).
[17] Y. Tanimura, D. Lacroix, and G. Scamps, Phys. Rev. C **92**, 034601 (2015).
[18] Y. Tanimura, D. Lacroix, and S. Ayik, Phys. Rev. Lett. **118**, 152501 (2017).
[19] G. Scamps, C. Simenel, and D. Lacroix, Phys. Rev. C **92**, 011602(R) (2015).
[20] C. Simenel and A. S. Umar, Phys. Rev. C **89**, 031601(R) (2014).
[21] B. D. Wilkins, E. P. Steinberg, and R. R. Chasman, Phys. Rev. C **14**, 1832 (1976).
[22] N. Carjan, F. A. Ivanyuk and Yu. Ts. Oganessian, J. Phys.: Conf. Ser. **863**, 012044 (2017).
[23] H. Pasca *et al.*, Nucl. Phys. A **969**, 226 (2018).
[24] Y. Abe, C. Gregoire, and H. Delagrange, J. Phys. **C47**, 4 (1986).
[25] T. Wada, Y. Abe, and N. Carjan, Phys. Rev. Lett. **70**, 3538 (1993).
[26] Y. Abe, S. Ayik, P-G. Reinhard, and E. Suraud, Phys. Rep. **275**, 49 (1996).
[27] P. Fröbrich and I. I. Gontchar, Phys. Rep. **292**, 131 (1998).
[28] G. D. Adeev *et al.*, Phys. Part. Nuclei **36**, 378 (2005).
[29] V. Zagrebaev and W. Greiner, Phys. Rev. C **78**, 034610 (2008).
[30] A. V. Karpov and V. V. Saiko, Phys. Rev. C **96**, 024618 (2017).
[31] P. Fröbrich and R. Lipperheide, *Theory of Nuclear Reactions* (Clarendon, Oxford, 1996); H. Krappe and K. Pomorski, *Theory of Nuclear Fission* (Springer, Berlin, 2012).
[32] C. Schmitt *et al.*, Acta Phys. Pol., B **34**, 1651 (2003).
[33] T. Asano, T. Wada, M. Ohta, T. Ichikawa, S. Yamaji, and H. Nakahara, J. Nucl. Radiochem. Sci. **5**, 1 (2004).
[34] T. Asano *et al.*, Prog. Theor. Phys. Suppl. **154**, 457 (2004).
[35] Y. Aritomo and S. Chiba, Phys. Rev. C **88**, 044614 (2013).
[36] Y. Aritomo, S. Chiba, and F. Ivanyuk, Phys. Rev. C **90**, 054609 (2014).
[37] J. Sadhukhan, W. Nazarewicz, and N. Schunck, Phys. Rev. C **93**, 011304(R) (2016).
[38] M. D. Usang, F. A. Ivanyuk, C. Ishizuka, and S. Chiba, Phys. Rev. C **94**, 044602 (2016).
[39] M. R. Pahlavani and S. M. Mirfathi, Eur. Phys. J. **52**, 95 (2016).
[40] M. R. Pahlavani and S. M. Mirfathi, Phys. Rev. C **96**, 014606 (2017).
[41] A. J. Sierk, Phys. Rev. C **96**, 034603 (2017).
[42] J. Sadhukhan, C. Zhang, W. Nazarewicz, and N. Schunck, Phys. Rev. C **96**, 061301(R) (2017).
[43] M. D. Usang, F. A. Ivanyuk, C. Ishizuka, and S. Chiba, Phys. Rev. C **96**, 064617 (2017).
[44] C. Ishizuka, M. D. Usang, F. A. Ivanyuk, J. A. Maruhn, K. Nishio, and S. Chiba, Phys. Rev. C **96**, 064616 (2017).
[45] F. P. Hessberger, Eur. Phys. J. A **53**, 75 (2017).
[46] R. Léguillon *et al.*, Phys. Lett. B **761**, 125 (2016).
[47] K. Hirose *et al.*, Phys. Rev. Lett. **119**, 222501 (2017).
[48] J. Maruhn and W. Greiner, Z. Phys. **251**, 431 (1972).
[49] K. Sato, A. Iwamoto, K. Harada, S. Yamaji, and S. Yoshida, Z. Phys. A **288**, 383 (1978).
[50] S. Yamaji, H. Hofmann, and R. Samhammer, Nucl. Phys. A **475**, 487 (1988).
[51] K. Hirose *et al.* (unpublished).
[52] See Supplemental Material at http://link.aps.org/supplemental/10.1103/PhysRevC.99.051601 for ϵ values and variation of the TKE dostribution with ϵ.
[53] H. J. Krappe, J. R. Nix, and A. J. Sierk, Phys. Rev. C **20**, 992 (1979).

[54] V. M. Strutinsky, Nucl. Phys. A **95**, 420 (1967).
[55] V. M. Strutinsky, Nucl. Phys. A **122**, 1 (1968).
[56] A. V. Ignatyuk, G. N. Smirenkin, and A. S. Tishin, Sov. J. Nucl. Phys. **21**, 255 (1975).
[57] J. E. Gindler, K. F. Flynn, L. E. Glendenin, and R. K. Sjoblom, Phys. Rev. C **16**, 1483 (1977).
[58] K. F. Flynn *et al.*, Phys. Rev. C **5**, 1725 (1972).
[59] D. C. Hoffman, J. B. Wilhelmy, J. Weber, W. R. Daniels, E. K. Hulet, R. W. Lougheed, J. H. Landrum, J. F. Wild, and R. J. Dupzyk, Phys. Rev. C **21**, 972 (1980).
[60] P. Möller, J. R. Nix, W. D. Myers, and W. J. Swiatecki, At. Data Nucl. Data Tables **59**, 185 (1995).
[61] R. L. Ferguson *et al.*, Phys. Rev. C **7**, 2510 (1973).
[62] C. Wagemans, E. Allaert, A. Deruytter, R. Barthelemy, and P. Schillebeeckx, Phys. Rev. C **30**, 218 (1984).
[63] J. Weber *et al.*, Nucl. Phys. A **221**, 414 (1974).
[64] M. Hunyadi *et al.*, Phys. Lett. B **505**, 27 (2001).
[65] K. Nishio *et al.*, Phys. Rev. C **67**, 014604 (2003).
[66] A. Bulgac *et al.*, Phys. Rev. Lett. **116**, 122504 (2016).
[67] M. D. Usang *et al.*, Sci. Rep. **9**, 1 (2019).